
Article:
Fujita, Nobuyuki, Hasnip, Philip James orcid.org/0000-0002-4314-4093, Probert, Matthew Ian James orcid.org/0000-0002-1130-9316 et al. (1 more author) (2015) Theoretical study of core-loss electron energy-loss spectroscopy at graphene nanoribbon edges. Journal of physics : Condensed matter. 305301. ISSN 1361-648X

https://doi.org/10.1088/0953-8984/27/30/305301

Theoretical study of core-loss electron energy-loss spectroscopy at graphene nanoribbon edges

N Fujita,* P J Hasnip, M I J Probert,† and J Yuan

Department of Physics, University of York,

Heslington, York, YO10 5DD, U.K.

(Dated: May 27, 2015)

Abstract

A systematic study of simulated atomic-resolution Electronic Energy-Loss Spectroscopy (EELS) for different graphene nanoribbons (GNRs) is presented. The results of *ab initio* studies of carbon $1s$ core-loss EELS on GNRs with different ribbon edge structures and different hydrogen terminations show that theoretical core-loss EELS can distinguish key structural features at the atomic scale. In addition, the combination of polarized core-loss EELS with symmetry resolved electronic partial density of states (PDOS) calculations can be used to identify the origins of all the primary features in the spectra. For example, the nature of the GNR edge structure (armchair, zigzag, etc) can be identified, along with the degree of hydrogenation. Hence it is possible to use the combination of *ab initio* calculations with high resolution, high energy transmission core-loss EELS experiments to determine the local atomic arrangement and chemical bonding states (i.e. a structural fingerprint) in GNRs, which is essential for future practical applications of graphene.

PACS numbers: 73.22.Pr,74.20.Pq,79.20.Uv

*Simulation and Analysis R&D Center, Canon Inc. 30-2, Shimomaruko 3-chome, Ohta-Ku, Tokyo 146-8501, Japan

†Author to whom correspondence should be addressed

I. INTRODUCTION

Graphene is an extraordinary material, comprising a single layer of carbon atoms, with remarkable properties, as noted in many recent review articles e.g. [1–4]. To fully utilize its electronic properties in device applications, there is a need to tailor the properties as the perfect infinite sheet is a semi-metal, and so some form of band-gap engineering is required. One very promising approach is to cut the sheet up into a graphene nanoribbon (GNR), which then opens up a width-dependent electronic energy band-gap [5]. The properties of GNRs are known to be sensitive to local atomic configurations [6, 7] and so elemental identification and electronic state analysis at the the atomic scale is becoming increasingly important. So far, the atomic configurations at graphene nanoribbon edges have been investigated by transmission electron microscopy [8, 9] and scanning probe techniques [10] but the electronic properties of the edge states has not yet been determined with atomic resolution.

Recently, there have been significant developments in energy-loss near-edge fine structure (ELNES) measurements, with a state-of-the art atomic resolution study of carbon $1s$ core-loss ELNES for different graphene nanoribbon edges reported by Suenaga and Koshino[11]. Such measurements required detailed theoretical modelling for a full understanding, and so in this work, a detailed study of the predicted ELNES spectra for various GNR edges and different hydrogen terminations is presented. This can then be used as a fingerprint for the interpretation of experimental ELNES measurements. ELNES is an example of Electron Energy Loss Spectroscopy (EELS) - hence all the comments here apply to the general EELS approach. However, it should be noted that in this work the focus is on high energy transmission EELS. If elastic scattering effects are properly taken into account, then EELS spectra taken in strong diffraction conditions (including those of the reflection EELS geometry) could also be taken into account, but that is beyond the scope of the current study. The carbon $1s$ core-losses can be easily distinguished from the low energy losses associated with both single particle and collective excitations of the valence electrons because they occur at different energies. Finally, in transmission EELS it is possible to perform the EELS measurements either in spatially or momentum-resolved modes wherein the momentum transfer wavevector $\mathbf{q}$ is analogous to the polarization vector in X-ray absorption spectra. Using differential methods[12, 13], the effect of the orientation of the polarization vector on the

EELS spectra can be studied with a highly localized probe, with nanometer resolution.

II. METHOD

Ab initio calculations of the electronic structure of various GNRs were performed using the CASTEP [14, 15] plane-wave DFT [16] code. The LDA exchange-correlation functional[17] was used, as that gives excellent structures for graphene materials without needing any extra dispersion correction. The simulation of an isolated GNR was achieved by using the supercell approach, with rigorous tests to make sure that the calculated EELS spectra were fully converged w.r.t. parameters such as periodic distance (the core-hole has a finite range, and to simulate an isolated core-hole requires a sample size of at least 8 Å in-plane direction), and the vacuum gap (the higher energy orbitals can be quite diffuse and give rise to spurious features in the EELS spectra unless the inter-layer separation is at least 14 Å). Brillouin zone sampling was done using Monkhorst-Pack grids with a sample density of $0.02 \times 2\pi\text{Å}^{-1}$. See the Supplementary Information for more details.

A specially constructed double-projector norm-conserving pseudopotential was used, with a $1s$ core-hole on one atom, using the "on-the-fly" methodology within CASTEP which is necessary for the core-states to be fully reconstructed in order to calculate the core-loss EELS spectra. The spectra plotted correspond to the modulus-squared of the dipole transition matrix elements,

$$I(E) = \sum_{\mathbf{k}} \omega_{\mathbf{k}} \sum_{n} \gamma\left(E - E_{n,\mathbf{k}}\right) \left|\langle\phi_c| r_\alpha |\psi_{n,\mathbf{k}}\rangle\right|^2 \tag{1}$$

where the summation is over unoccupied states n and Brillouin zone sample points $\mathbf{k}$ with weights $w_{\mathbf{k}}$, $|\phi_c\rangle$ is the core state on the site of interest and $|\psi_{n,\mathbf{k}}\rangle$ is a (single particle) conduction state. Finally, due to the limited number of sampling points, a Lorentz broadening function $\gamma\left(E - E_{n,\mathbf{k}}\right)$ was incorporated into the Brillouin zone spectral integration. Full details on the pseudopotential core-loss EELS methodology are in ref. [18]. Additional details on the calculations and data such as convergence with ribbon width are included in the Supplemental Material.

The structures considered were all electrically neutral, and so the following simple expression was sufficient to define the formation energy of the two edges of the graphene nanoribbon E_{edge}^{GNR}:

$$E_{edge}^{GNR} = \frac{E_{total}^{GNR} - N_C\mu_C - N_H\mu_H}{N_C^{edge}} \quad (2)$$

where N_c is the total number of carbon atoms in the ribbon, N_c^{edge} is the number of carbon atoms at the two edges of the ribbon, N_H is the number of passivation hydrogen atoms added in total at both edges, E_{total}^{GNR} is the electronic total energy of the ribbon containing $N_C + N_H$ atoms, μ_C is the chemical potential of carbon and μ_H is the chemical potential of hydrogen. The carbon atoms are assumed to come from a reservoir of graphene, and so $\mu_C = \frac{E_{total}^{graphene}(N)}{N}$ for a graphene unit cell of N carbon atoms. For hydrogen, the reservoir is assumed to be molecular gas and so $\mu_H = \frac{E_{total}^{H2}}{2}$. Note that by common convention, the ribbon edge formation energy is normalized by the number of atoms in the edge and not by the length of the edge; hence it has dimensions of energy, unlike the usual convention for a surface energy which is normalized by the area of the surface.

A. Structures - atomistic and magnetic

The study of GNRs usually focuses on two basic classes: armchair (AGNR) and zigzag (ZGNR), with varying degrees of edge hydrogenation (i.e. none, one hydrogen (+1 H) or two hydrogen (+2 H) per edge carbon atom). The hydrogen acts to electronically passivate any dangling edge states. For a ZGNR there is an additional possibility of a self-passivated state – the zigzag edge reconstruction (zz-57) – in which 2 adjoining hexagons at the zigzag edge reconstruct into a pentagon and a heptagon. This has been shown[19] to be the more favoured edge of ZGNR in the absence of hydrogen. It should be noted that the unreconstructed ZGNR corresponds to a local energy minimum and is metastable, and that there is an energy barrier between this and the reconstructed zz-57 structure, which is why it was not discovered for a long time.

In this work, a third basic possibility was also considered, which is the less commonly studied Klein edge[20], which has a carbon atom with a single bond to the rest of the ribbon, and which can be passivated with up to +3 H per edge carbon atom.

For each GNR, full structural relaxation of all the atoms (including any edge hydrogens) was performed and the electronic structure evaluated with and without an explicit treatment of spin polarization. It was found that the only GNR structure with a significant spin moment was the unhydrogenated, unreconstructed ZGNR - the addition of +1H reduced the

spin moment significantly, and +2H quenched it altogether, as shown in figure 1. A detailed study of the corresponding core-loss EELS showed no discernible change with/without spin polarization, and no significant spin moment was found in any other GNR structures, and so spin effects are neglected for the remainder of this paper.

B. Core-loss EELS spectra

With a pseudopotential-based method, the core states were reconstructed using a PAW method as described in [18]. The transition energy is the difference between the binding energy of the core electrons and the energy of the excited electrons, the accurate calculation of which requires consideration of many-body effects and is beyond the scope of the current work. Here the focus was on the spectral variation near the onset of the core electron excitation and so the energies of the spectra were shifted by the onset energy, which is of the order of the core states involved (i.e. around 285 eV for C 1s electron excitation spectroscopy such as considered here), so that in all the results presented here the 1s-edge onset is at 0 eV. The general accuracy of this method within CASTEP has been rigorously evaluated and compared to a more traditional all-electron approach and found to produce very similar results at much reduced computational cost[21]. For the particular case of carbon polymorphs, the accuracy of DFT calculated EELS compared to experiments has also been demonstrated [22].

For each structure considered, the carbon 1s core-loss EELS spectrum was calculated up to 60 eV above the onset, and then normalized so that the integrated area from 0-60 eV was unity. By selecting different sites for the core-hole, it is possible to generate an atom-resolved core-loss EELS, which is the level of spatial resolution that is now becoming experimentally available. It is also possible to average the different site-resolved spectra, with appropriate weighting for the number of different equivalent sites, to generate a total spectrum representing a low-spatial resolution experiment, being the core-loss EELS for the total ribbon.

III. RESULTS

A. Edge Formation Energies

There is a small variation in the edge formation energy with GNR width, with reasonable convergence for widths greater than 8 Å wide. The Klein-edge structure is unstable without any hydrogen passivation, with a reconstruction to a structure with two neighbouring edge carbon atoms bonding to make a 5-member ring. With hydrogen passivation, the Klein edge is a local energy minimum without a significant carbon reconstruction. Both AGNR and ZGNR are unable to accept +3 H per edge carbon atom.

The edge formation energy for all the fully relaxed edge structures considered are included in table I. This shows that for both ZGNR and AGNR the most stable edge has +2 H per edge carbon atom, whilst the Klein edge is most stable when it has +3H per edge carbon atom. The large negative formation energies for AGNR+2H shows that this edge is unequivocally thermodynamically stable and can spontaneously form. The small energies for AGNR+H and ZGNR+2H suggest that they are probably stable at room temperature, whilst the larger positive values for all the other edges suggest these edge are metastable, and may only be stable in vacuum or a very low hydrogen content environment. All of these structures have been seen experimentally[8, 10, 23].

B. Core-loss EELS Spectra

1. Armchair Graphene Nano-Ribbons

The calculated core-loss EELS for an unhydrogenated (unpassivated) AGNR is shown in figure 2. There are four distinct peaks visible, labelled P1 ... P4, whose identity can be determined by considering polarized core-loss EELS.

A perfect graphene sheet has higher symmetry than a GNR, and consequently if the applied electric field is polarized in the plane of the sheet (either X- or Y-direction here) then transitions into the anti-bonding states of σ^*-symmetry are allowed, but with Z-direction polarization then transitions into the anti-bonding states of π^*-symmetry are allowed. Hence by calculating the effect of different E-field polarizations on the core-loss EELS for a unhydrogenated AGNR as shown in figure 3, the origins of the main peaks can be determined.

This shows that the dominant contribution to peak P1 is from the edge carbon atom (site 1) with the X-direction polarization and is consistent with the site-resolved core-loss EELS shown in figure 2. This is the only site in AGNR that has triple bonds, and therefore this peak can be assigned to the transition into the anti-bonding π^* state of the triple bonds in X-Y plane. The P2 peak is present in the spectra of each atom and appears in the Z-direction and may therefore be assigned to the out-of-plane π^* state. Similarly, P3 and P4 mainly appear in the X- and Y-directions respectively, and can be assigned to in-plane σ^* states. In particular, P3 has a dominant contribution from interchain bonds (i.e. bonds that are perpendicular to the GNR edge) and P4 from intrachain bonds (i.e. bonds that are parallel to the GNR edge).

In the same way, the effect of progressively increasing levels of hydrogenation (either 0, +1 H or +2 H per edge C atom) on the AGNR are shown in figure 4. The dominant σ^* and π^* peaks are easily visible, but there are clearly additional peaks that depend upon the degree of hydrogenation. This clearly shows the power of core-loss EELS to identify subtle structural differences. Note that hydrogen is usually very hard to detect in most forms of electron microscopy, and so this is an additional advantage to this approach - it is possible to identify the binding site and number of hydrogen atoms present.

A study of the sources of the difference in the core-loss EELS with hydrogenation is also possible by considering the site- and symmetry-resolved spectra. Figure 5 shows the atom-resolved core-loss EELS for a mono-hydrogenated (+1 H) AGNR. Clearly there is a new peak that is visible when the core-hole is on the edge carbon atom, that is not present in the unhydrogenated AGNR, which can therefore be assigned to the C-H bond. The polarized E-field results shown in figure 6 confirms this suspicion - the new peak is visible in the X- and Y- directions but not Z, which proves that it is due to the C-H bond.

Finally, the projected electronic density of states (PDOS) for the edge carbon atom is shown in figure 7, along with the corresponding core-loss EELS. It is well known that the core-loss EELS depends upon the PDOS, but the symmetry resolution (projection onto angular momentum states) confirms the intuition that this extra peak is due to a transition to a σ^* state for the C-H bond. In general, the dipole selection rule suggests that only p-states need to be considered, and for low energies (below 3 eV), figure 7 confirms that this is the dominant component of the core-loss EELS and hence only transitions to anti-bonding π^* states are possible. At higher energies, e.g. above 3 eV, there is evidence of s-p

hybridization and transitions to σ^* states become possible. Note that the extra peak is seen in both X- and Y- directions and so is due to the σ^* state for the edge carbon atom, which has been red-shifted by about 4.7 eV compared to the other carbon atoms due to the longer C-C bond length for the edge atom.

Hence by combining symmetry-resolved PDOS and the polarized atom-resolved core-loss EELS it is possible to identify the detailed origins of the different peaks, which therefore underlines the usefulness of *ab initio* calculations for core-loss EELS studies.

A similar picture emerges from the study of the di-hydrogenated (+2 H) AGNR. As can be seen in figure 8, the key difference is that there are now two C-H bonds per edge carbon which are out of the plane of the GNR. Comparison of the total spectrum with figure 4 shows that there are now two additional peaks (labelled A1 and A2) compared to the unhydrogenated AGNR. The site-resolved core-loss EELS shows that the key difference is in the spectrum associated with the edge carbon atom. The polarized core-loss EELS in figure 9 shows that A2 is associated with the Z-direction and A1 (which is actually a double peak) with the X- and Y- directions. Also, the low-energy π^* state is missing for site 1. This can be understood as the two C-H bonds are out of the plane of the AGNR which therefore suppresses the transition to the π^* state at this site. The A1 peak is a double peak, due to the two C-H bonds, but in the total spectrum the lower peak of the doublet merges into the shoulder of the dominant π^* peak. Hence A1 is due to a transition to the σ^* state for the C-H bond. The A2 peak is seen in both X- and Y- directions and so is due to the σ^* state for the edge carbon atom, which has been red-shifted by about 2.9 eV compared to the other carbon atoms. This shift is due to the longer C-C bond length for the edge carbon due to the hydrogen saturation for this atom. The shift for the A2 peak is less than that for the A1 peak due to the level broadening caused by the two σ^* states.

2. Zigzag Graphene Nano-Ribbons

The site-resolved core-loss EELS for the unhydrogenated and unreconstructed ZGNR is shown in figure 10. As expected, the edge carbon atom is qualitatively different to the other sites. However, whilst this structure is mechanically stable, it has a higher energy than the reconstructed zz-57 structure, and so it is the reconstructed structure that will later be studied in more detail. Note that the edge atom (site 1) has a very strong π^*

peak, due to the unoccupied edge state, which is the origin of the unpaired spin density and the AFM signature seen in figure 1. This state is rapidly suppressed by reconstruction or hydrogenation (see below) which explains why AFM is not routinely observed in GNRs.

The site-resolved core-loss EELS for the reconstructed zz-57 structure (which is energetically more stable than the unhydrogenated and unreconstructed ZGNR structure in figure 10) is shown in figure 11. This structure has considerably lower symmetry than the simpler unreconstructed one, and consequently there are many more distinct sites to consider. The total core-loss EELS has four distinct peaks, labelled S1 ... S4 to be considered. Once again, consideration of the site-resolved spectra, in combination with the polarized core-loss EELS in figure 12, enables the peaks to be identified. Peak S1 is clearly the transition to the anti-bonding π^* state of the triple bonds of the reconstructed edge atoms as it is very strong in the X-direction. Peak S2 is found in the Z-direction for all the core-hole sites and so corresponds to a π^* peak. Peak S3 is strong in the X-direction, whilst S4 is strong in the Y-direction (particularly for the inner carbon atoms 4-7) and so both can be assigned to σ^* states.

The effect of hydrogenation on the ZGNR can be seen in figure 13. As with the AGNRs, there are distinct new features that can be seen upon the addition of hydrogen to the edge atoms. Note that the "non-passivation" spectrum is that for the unreconstructed ZGNR - this is so that the effect of hydrogen on the spectrum is clearer, as there is only a small change in the carbon atom positions upon hydrogenation. The reconstructed zz-57 GNR is more stable, but is unable to accept any hydrogen at all as there are no unpaired electrons at the edge sites. Hence whilst the zz-57 GNR structure is more stable than unreconstructed ZGNR in the absence of hydrogen, it can be seen from the results in table I that the situation is reversed in the presence of hydrogen.

A detailed study of the changes in the core-loss EELS upon hydrogen passivation can also be performed for ZGNR structures. The effect of mono-hydrogenation can be seen in figure 14 which clearly shows an additional peak (labelled M) that can be seen in the total core-loss EELS. On this occasion, it is not so obvious which site makes the dominant contribution to this peak, although there is a clear reduction in the low-energy π^* peak due to the elimination of the unoccupied edge state. Close examination of the polarized core-loss EELS in figure 15 and the corresponding PDOS plot in figure 16 show that it is dominated by an X-direction component from site 1, and from a Z-direction component from all sites.

Hence this peak cannot be attributed to a pure σ^*(C-H) peak (unlike the corresponding situation in AGNRs) but also contains a contribution from π^* state for all carbon atoms in the ribbon. This is confirmed by the PDOS plot showing strong contribution from both s- and p-states around 5 eV.

A similar picture is seen for the fully (di-)hydrogenated ZGNRs. As shown in figure 17, there are now two new peaks, labelled D1 and D2, that are not present in the unhydrogenated ZGNR, and associated with the edge carbon atom (site 1). Consideration of the site-resolved polarized core-loss EELS spectra in figure 18 suggests that whilst D2 seems to be a pure π^* peak as it only appears in the Z-direction, the situation is more complex for the D1 peak. D1 is dominated by a σ^*(C-H) peak (site 1, X-direction) but there is also a small component from the other carbon sites (Z-direction). This implies that there is some hybridization between the σ^*(C-H) state and a π^* state, which is therefore the origin of the energy difference between D1 and D2.

3. Klein-edge Graphene Nano-Ribbons

The final GNR to consider is the Klein edge structure. This structure is less commonly studied than AGNR and ZGNR, but as shown in table I, it can be energetically competitive with both AGNR and ZGNR structures. It can be considered as the addition of an extra carbon atom to a ZGNR edge, and as such has 3 unpaired electrons and hence is very reactive. The mono- and di-hydrogenated structures are qualitatively similar to the previous hydrogenated structures reported above, so only the most stable state, the tri-hydrogenated (+3 H) one, is reported here. The site-resolved and total core-loss EELS are shown in figure 19 and the corresponding polarized core-loss EELS in figure 20. Two qualitatively new peaks can be seen, labelled K1 and K2, that are associated with the edge carbon site. Once again, the edge π^* peak is not present because this carbon atom is sp^3-bonded to three hydrogen atoms and one other carbon atom. The K1 peak has an X-Y component from site 1 and also a significant Z-component from all the carbon atoms, and hence is assigned to a mixture of π^* and the σ^*(C-H) bond. The K2 peak is almost entirely due to site 1 and the Z-direction and is therefore associated with a π^*(C-H) bond.

IV. DISCUSSION AND CONCLUSIONS

Atomic resolution core-loss EELS has been achieved experimentally [11] and used to study graphene edges. The advantage of the *ab initio* approach to core-loss EELS is that it is possible, via a combination of analyses as demonstrated above, to accurately reproduce and understand the experimental spectra. In an anisotropic material such as a GNR, the use of polarized core-loss EELS is a very useful source of extra spatial information, and combined with symmetry resolved electronic PDOS, can be used to identify the origins of all the primary features. In this way, polarized atom-resolved core-loss EELS can be used as a fingerprint for structure determination.

As an example of the power of core-loss EELS as a fingerprint method, consider the case of carbon triple bonds: the first sharp peak at the edge carbon site in polarized core-loss EELS in the X-direction is a clearly identifiable feature seen in figures 3 and 12. Similarly, in the case of hydrogenation, the first sharp peak at the edge carbon atom in the X- and Y-directions can be readily identified in figures 6, 15, 20, etc.

From an experimental point of view, this combination of atomic-resolution and polarization presents a significant challenge. Atomic resolution core-loss EELS normally involves use of a convergent electron probe, but in that case the polarization information may be mixed, and instead separate polarization-dependent core-loss EELS measurements using a less convergent beam over a larger area is required. However, there is an alternative way of combining site-resolved and polarization-resolved core-loss EELS using two different convergence angles and use the difference signal to extract the anisotropic information [12, 13].

Finally, to summarize the key points about the core-loss EELS spectra for the different structures considered, the unpolarized core-loss EELS spectrum for a core-hole on the edge carbon atom is shown in figure 21. The spectra are arranged vertically in order of increasing energetic stability, with di-hydrogenated AGNR at the top, and unhydrogenated, unreconstructed ZGNR at the bottom. Whilst the general trends are clear, this also shows that peak position alone is insufficient to unambiguously identify the structure, and that the polarization analysis is an essential requirement.

Acknowledgments

NF gratefully acknowledges the support of Canon Inc, for an extended sabbatical to perform this research at the University of York, U.K. Computational resources were provided by the University of York, and by the UK national supercomputer, HECToR, as part of the UKCP consortium supported by EPSRC grant EP/F036884/1. MP, PH and JY gratefully acknowledge EPSRC funding that enabled this research.

---

[1] A. K. Geim, Science **324**, 1530 (2009).

[2] A. H. CastroNeto, F. Guinea, N. M. R. Peres, K. S. Novoselov, and A. K. Geim, Rev. Modern Phys. **81**, 109 (2009).

[3] S. DasSarma, S. Adam, E. H. Hwang, and E. Rossi, Rev. Modern Phys. **83**, 407 (2011).

[4] Y. Hancock, J. Phys. D-Applied Physics **44**, 473001 (2011).

[5] M. Y. Han, B. Oezyilmaz, Y. Zhang, and P. Kim, Phys. Review Letters **98**, 1229 (2007).

[6] F. Cervantes-Sodi, G. Csanyi, S. Piscanec, and A. C. Ferrari, Phys. Review B **77**, R16352 (2008).

[7] J. Kunstmann, C. Ozdogan, A. Quandt, and H. Fehske, Phys. Review B **83**, 1088 (2011).

[8] Z. Liu, K. Suenaga, P. J. F. Harris, and S. Iijima, Phys. Review Letters **102**, 2068 (2009).

[9] C. O. Girit, J. C. Meyer, R. Erni, M. D. Rossell, C. Kisielowski, L. Yang, C. H. Park, M. F. Crommie, M. L. Cohen, S. G. Louie, and A. Zettl, Science **323**, 1705 (2009).

[10] Y. Kobayashi, K. Fukui, T. Enoki, K. Kusakabe, and Y. Kaburagi, Phys. Review B **71**, R16352 (2005).

[11] K. Suenaga and M. Koshino, Nature **468**, 1088 (2010).

[12] Y. Sun and J. Yuan, Phys. Review B **71**, 465 (2005).

[13] X. R. Hu, Y. K. Sun, and J. Yuan, Ultramicroscopy **108**, 465 (2008).

[14] S. J. Clark, M. D. Segall, C. J. Pickard, P. J. Hasnip, M. J. Probert, K. Refson, and M. C. Payne, Z. Kristall. **220**, 567 (2005).

[15] V. Milman, K. Refson, S. J. Clark, C. J. Pickard, J. R. Yates, S. P. Gao, P. J. Hasnip, M. I. J. Probert, A. Perlov, and M. D. Segall, J. Molecular Structure-Theochem **954**, 22 (2010).

[16] P. J. Hasnip, K. Refson, M. I. J. Probert, J. R. Yates, S. J. Clark, and C. J. Pickard,

Philosophical Trans. Royal Soc. A-Mathematical Phys. Engineering Sciences **372**, 1473 (2014).

[17] J. P. Perdew and A. Zunger, Phys. Rev. B **23**, 5048 (1981).

[18] S. P. Gao, C. J. Pickard, M. C. Payne, J. Zhu, and J. Yuan, Phys. Review B **77**, 115122 (2008).

[19] P. Koskinen, S. Malola, and H. Hakkinen, Phys. Review Letters **101**, R16352 (2008).

[20] D. J. Klein, Chem. Phys. Letters **217**, 261 (1994).

[21] C. R. Seabourne, A. J. Scott, R. Brydson, and R. J. Nicholls, Ultramicroscopy **109**, 1374 (2009).

[22] S. P. Gao, J. Zhu, and J. Yuan, Chem. Phys. Letters **400**, 413 (2004).

[23] P. Koskinen, S. Malola, and H. Haekkinen, Phys. Review B **80**, 073401 (2009).

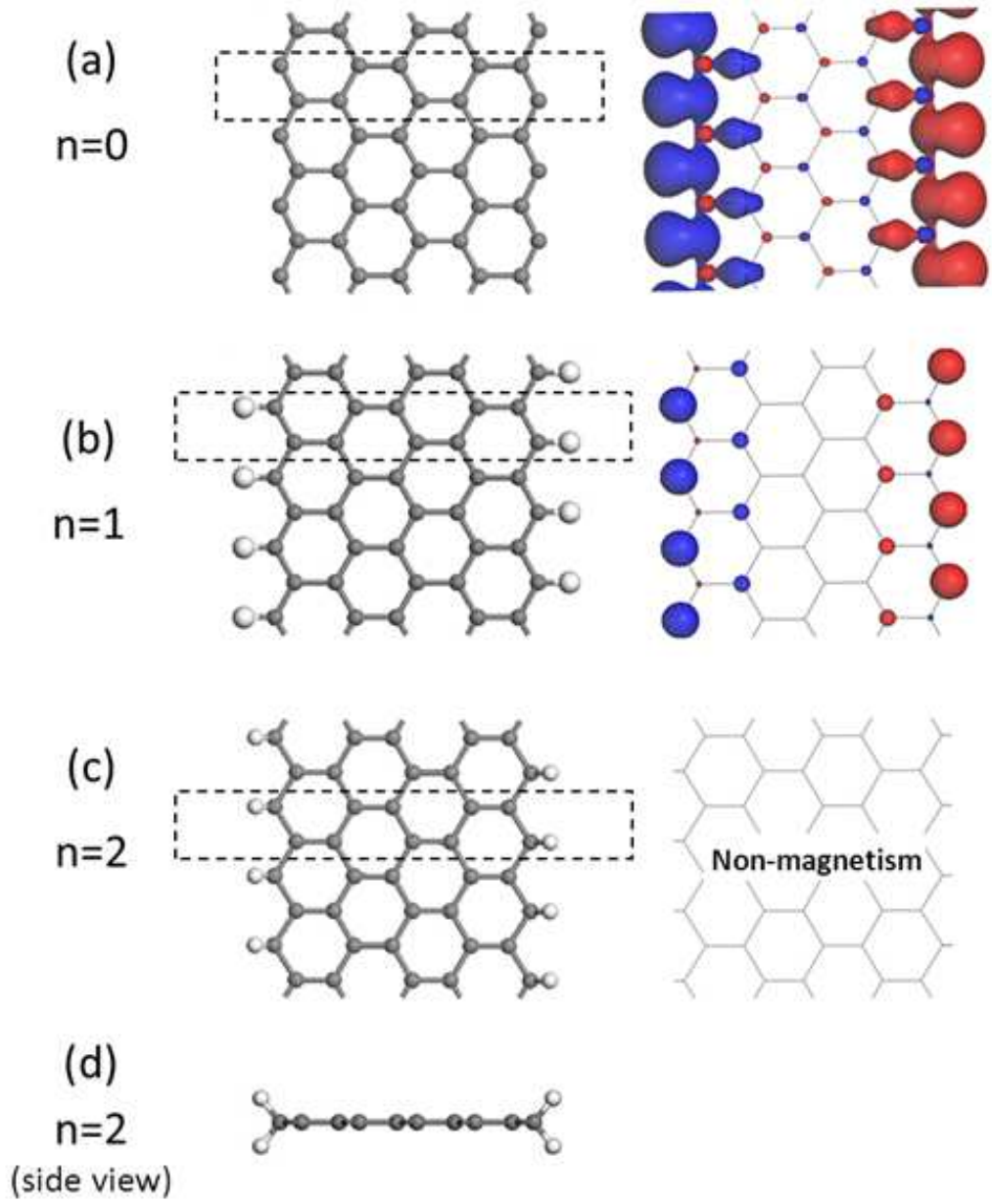

Figure 1: (Color online) (a) shows the unhydrogenated structure of an unreconstructed ZGNR on the left, and the spin density at isosurface 0.06 electrons/bohr^3. The red colour is for up (alpha) spin density and the blue for down (beta) spin. The structure is clearly anti-ferromagnetic. (b) shows the same but with the addition of +1H per edge carbon atom. The spin moment is significantly reduced. (c) shows the same but with +2 H per edge carbon and now the spin moment is zero at all points on the ribbon.

Table I: Summary of the edge formation energies. Smaller values are more energetically favoured.

Structure	Edge formation energy (eV)	
	This work	Koskinen *et al*[19]
ZGNR	3.469	3.22
Klein+H	2.928	
ZZ57	2.574	2.36
AGNR	2.287	2.09
Klein+2H	1.166	
Klein+3H	0.753	
ZGNR+H	0.223	
AGNR+H	0.050	
ZGNR+2H	-0.078	+0.15
AGNR+2H	-0.357	+0.02

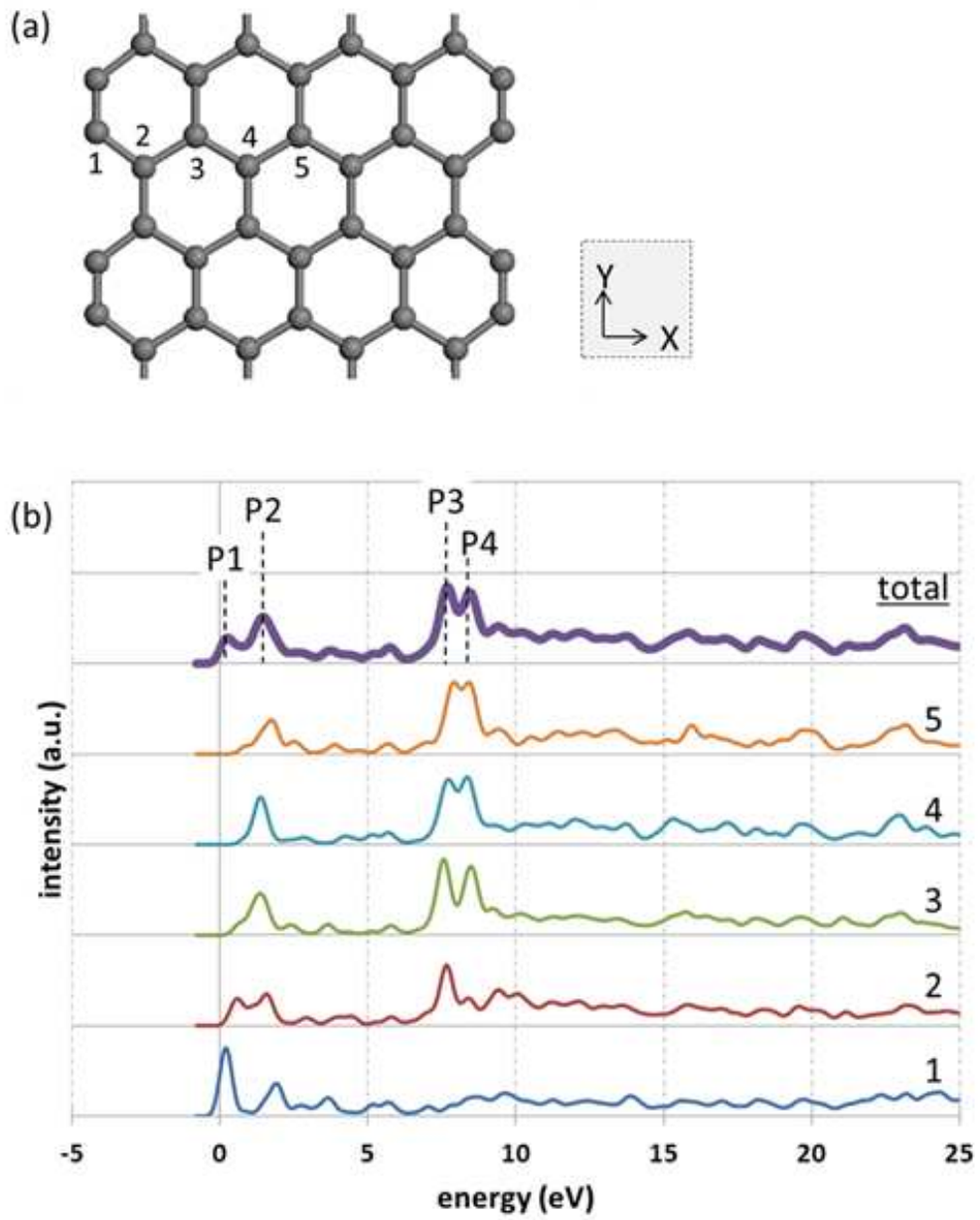

Figure 2: (Color online) Atom-resolved core-loss EELS for each of the distinct sites in an unhydrogenated AGNR. (a) shows the labeling of each site and the coordinate system used. (b) shows the calculated core-loss EELS for a core-hole on the labelled carbon atom, and "total" shows the effect of averaging the core-loss EELS across all sites. Four distinct peaks are visible, labelled P1 to P4 - see text for a discussion.

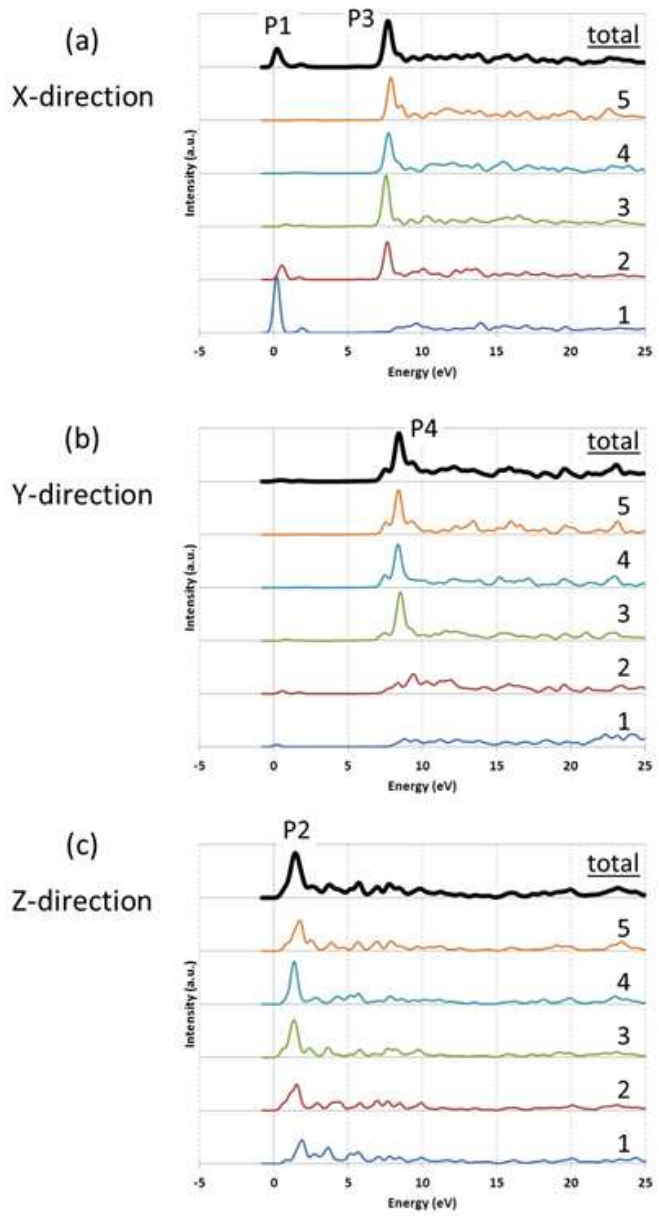

Figure 3: (Color online) Effect of polarized E-field on the atom-resolved core-loss EELS for each of the distinct sites in a unhydrogenated AGNR. (a) shows the effect of incident E-field that is polarized in the X direction, i.e. across the width of the ribbon. (b) shows the effect of Y-direction polarization, i.e. along the periodic direction of the ribbon. (c) shows the effect of Z-polarization, i.e. in the aperiodic direction perpendicular to the ribbon plane. The peak labeling is the same as in figure 2.

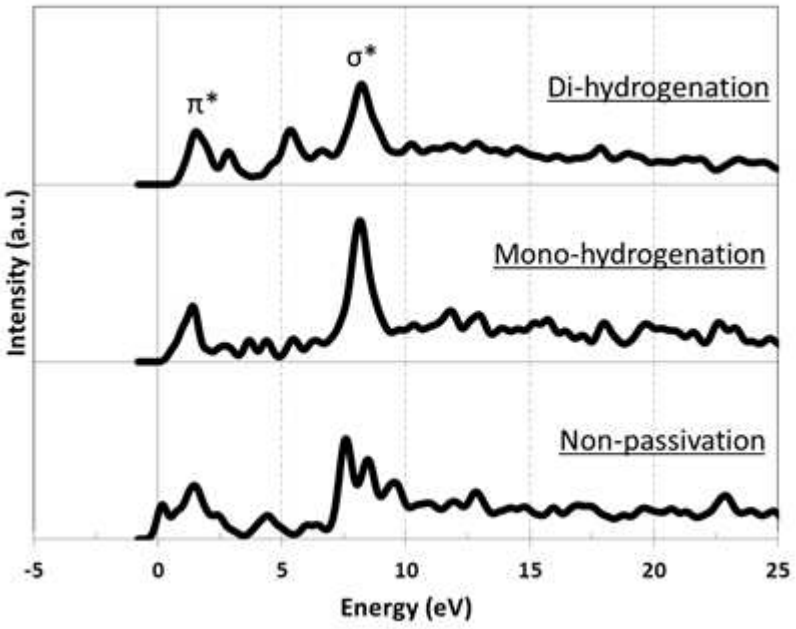

Figure 4: Effect of hydrogenation on the total core-loss EELS for an AGNR.

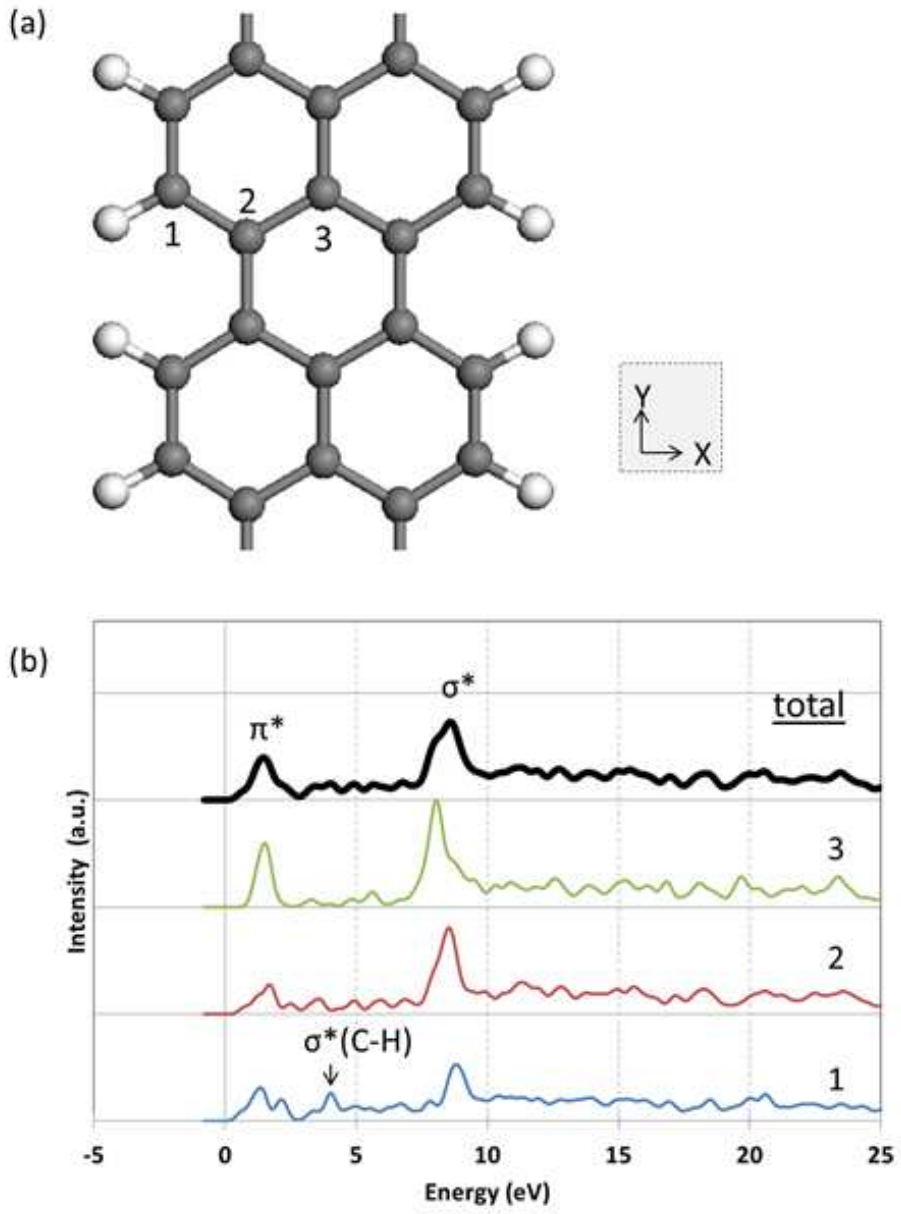

Figure 5: (Color online) Atom-resolved core-loss EELS for each of the distinct sites in a mono-hydrogenated AGNR. (a) shows the labeling of each site and the coordinate system used. (b) shows the calculated core-loss EELS for a core-hole on the labelled carbon atom, and "total" shows the effect of averaging the core-loss EELS across all sites. There is a qualitatively new peak visible in the core-loss EELS for site 1, that can therefore be attributed to the C-H bond that is found at this site and nowhere else in this AGNR.

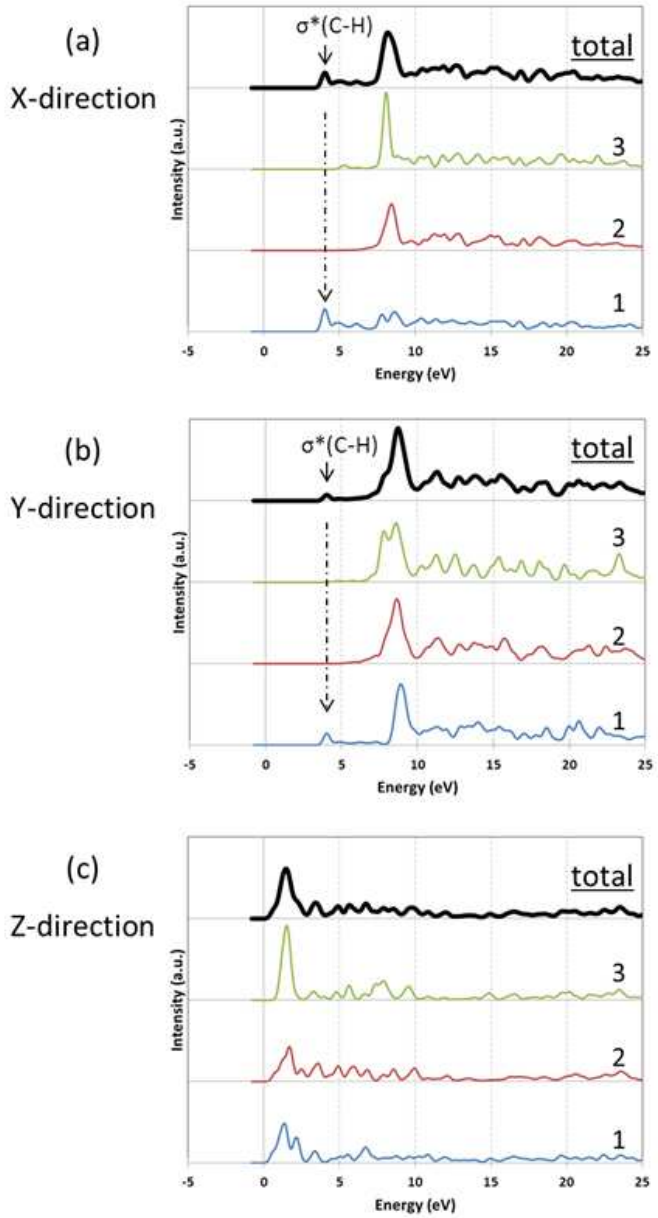

Figure 6: (Color online) Effect of polarized E-field on the atom-resolved core-loss EELS for each of the distinct sites in a mono-hydrogenated AGNR. Parts (a), (b) and (c) shows the effect of incident E-field that is polarized in the X-, Y- and Z- direction respectively. The new peak that is assigned to the C-H bond is highlighted. The site labeling is the same as in figure 5.

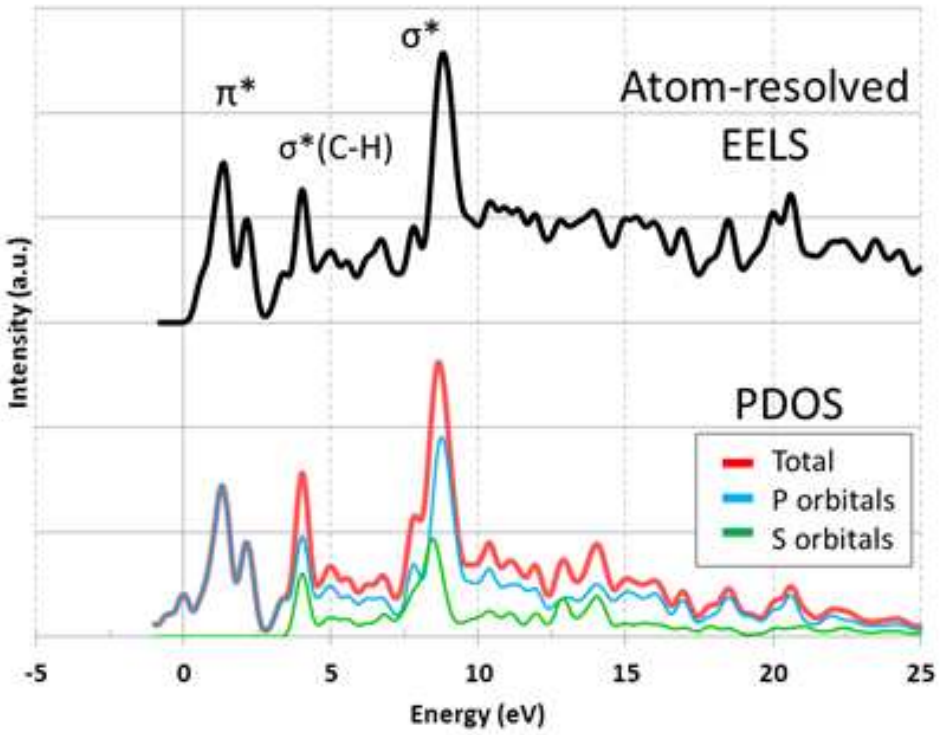

Figure 7: (Color online) Comparison of atom-resolved core-loss EELS (top) and the projected electronic density of states (bottom) for the edge site in mono-hydrogenated AGNR. The PDOS makes a dominant contribution to the core-loss EELS spectrum and helps with the assignment of the symmetry of each peak.

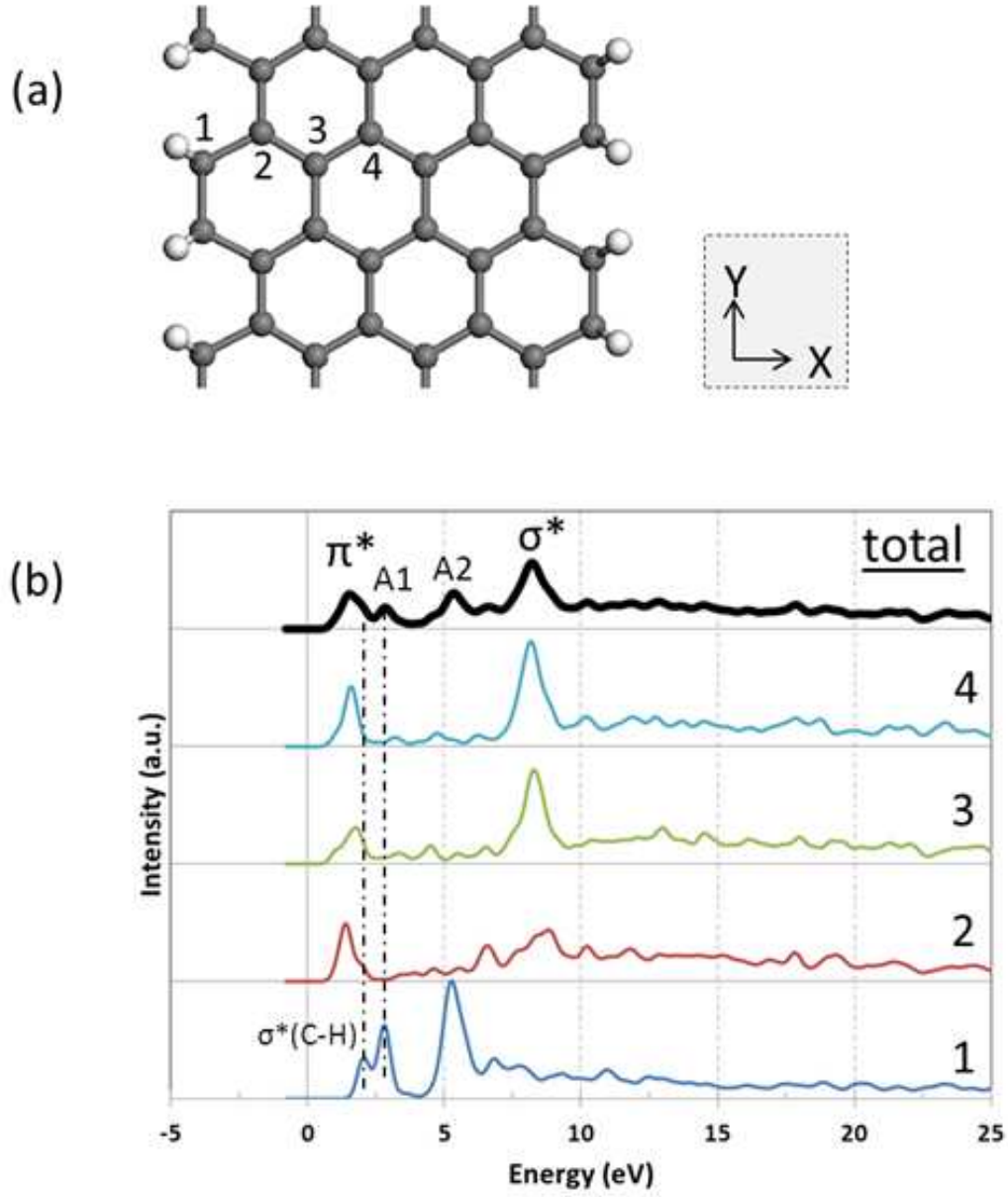

Figure 8: (Color online) Atom-resolved core-loss EELS for each of the distinct sites in a di-hydrogenated AGNR. (a) shows the labeling of each site and the coordinate system used. (b) shows the calculated core-loss EELS for a core-hole on the labelled carbon atom, and "total" shows the effect of averaging the core-loss EELS across all sites. There are two qualitatively new peaks visible in the core-loss EELS for site 1, labelled A1 and A2. See text for a detailed discussion of these peaks.

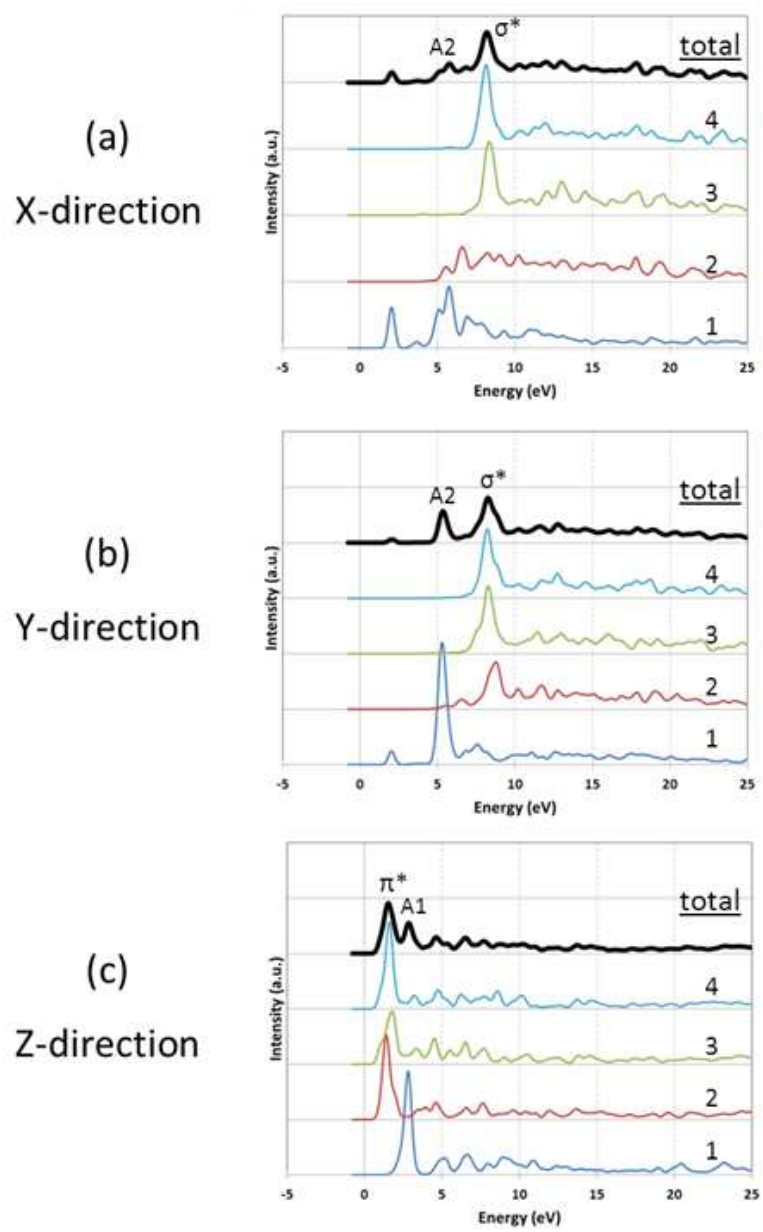

Figure 9: (Color online) Effect of polarized E-field on the atom-resolved core-loss EELS for each of the distinct sites in a di-hydrogenated AGNR. Parts (a), (b) and (c) shows the effect of incident E-field that is polarized in the X-, Y- and Z- direction respectively. There are two new peaks that are associated with the two C-H bonds. Peak A1 is seen in the Z-direction, and peak A2 in the X- and Y- directions. The site labeling is the same as in figure 8.

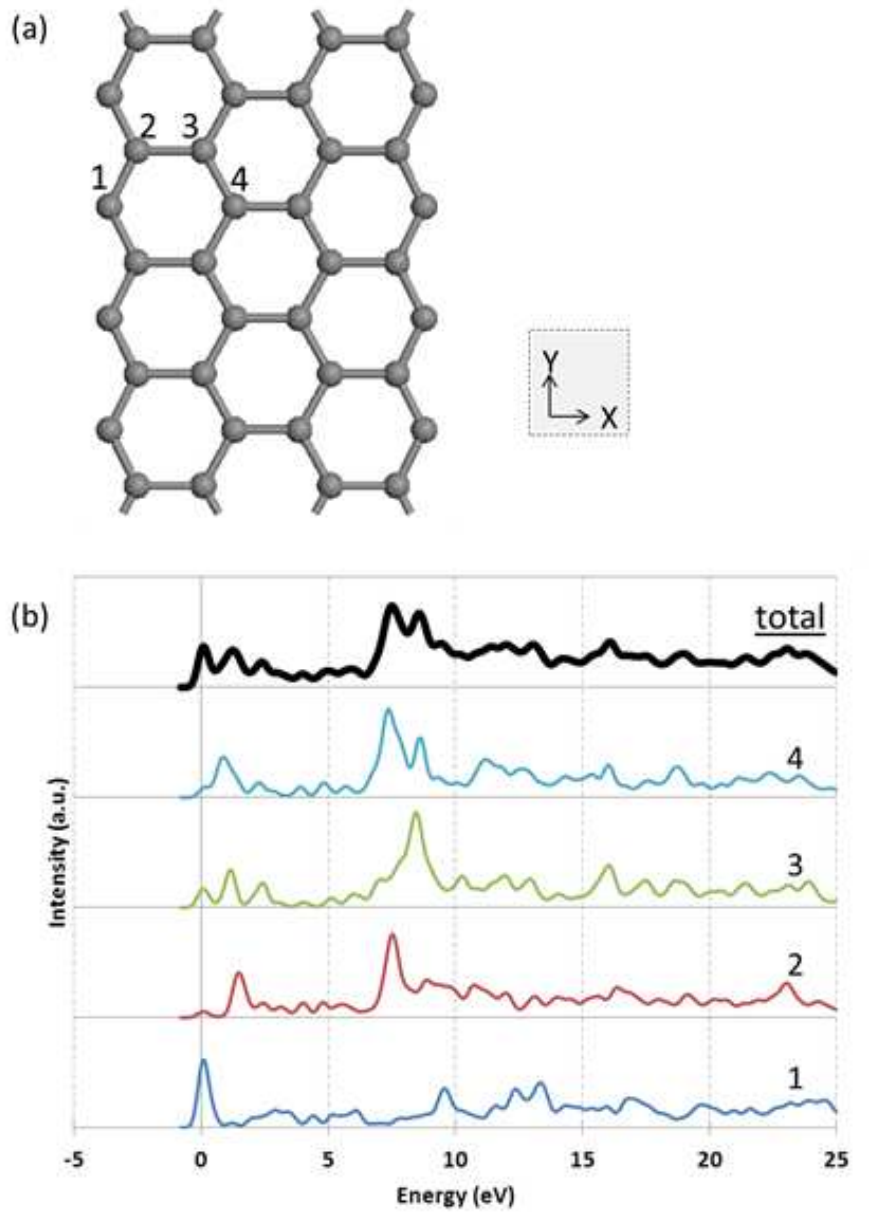

Figure 10: (Color online) Atom-resolved core-loss EELS for each of the distinct sites in a mono-hydrogenated AGNR. (a) shows the labeling of each site and the coordinate system used. (b) shows the calculated core-loss EELS for a core-hole on the labelled carbon atom, and "total" shows the effect of averaging the core-loss EELS across all sites.

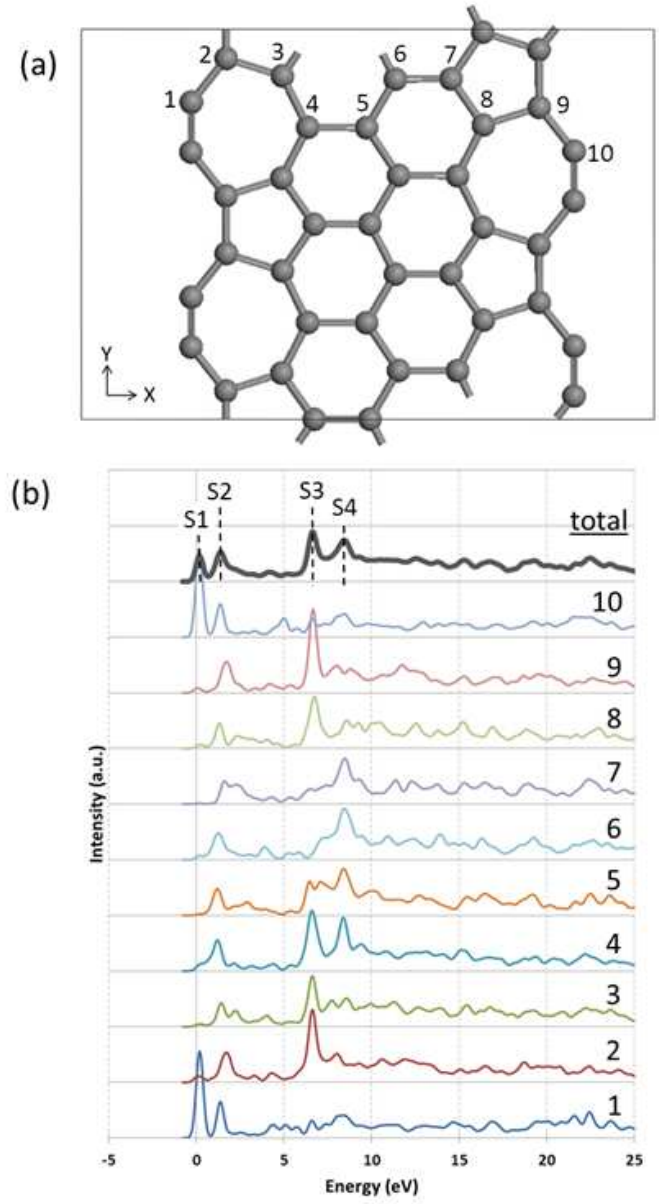

Figure 11: (Color online) Atomic sites resolved core-loss EELS for the reconstructed zz-57 GNR. There is a considerable symmetry lowering, and hence more distinct sites to consider. Four distinct peaks, labelled S1 ... S4 in the total core-loss EELS are visible. See text for a detailed discussion.

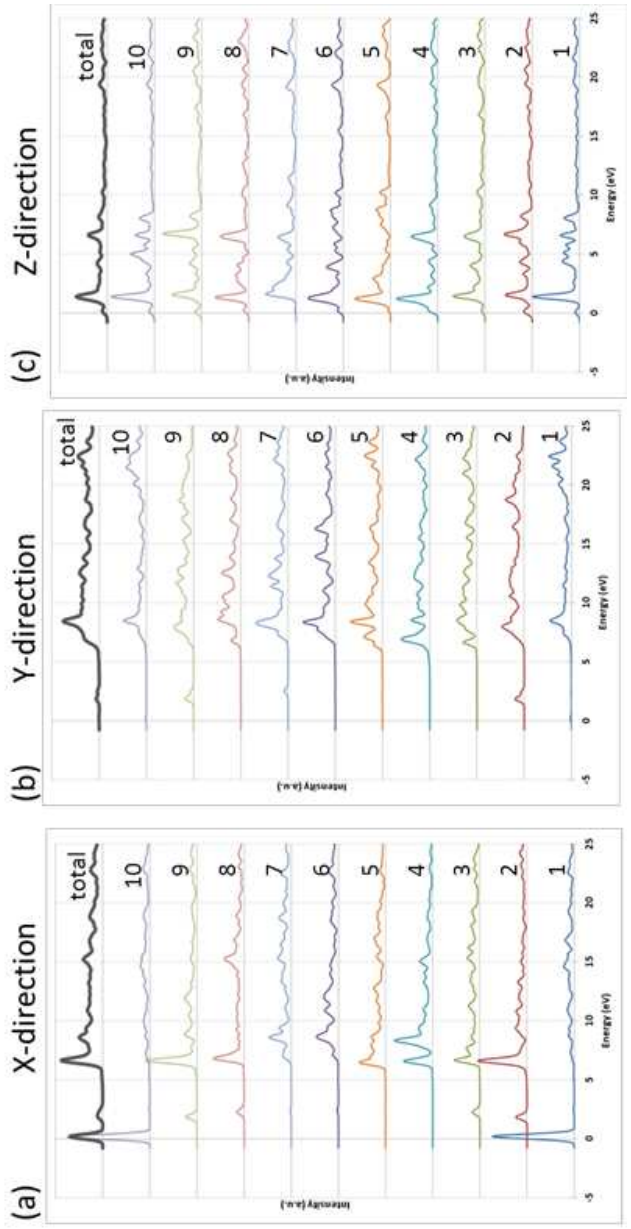

Figure 12: (Color online) Effect of polarized E-field on the atom-resolved core-loss EELS for each of the distinct sites in a reconstructed zz-57 GNR. Parts (a), (b) and (c) shows the effect of incident E-field that is polarized in the X-, Y- and Z- direction respectively. The site labeling is the same as in figure 11.

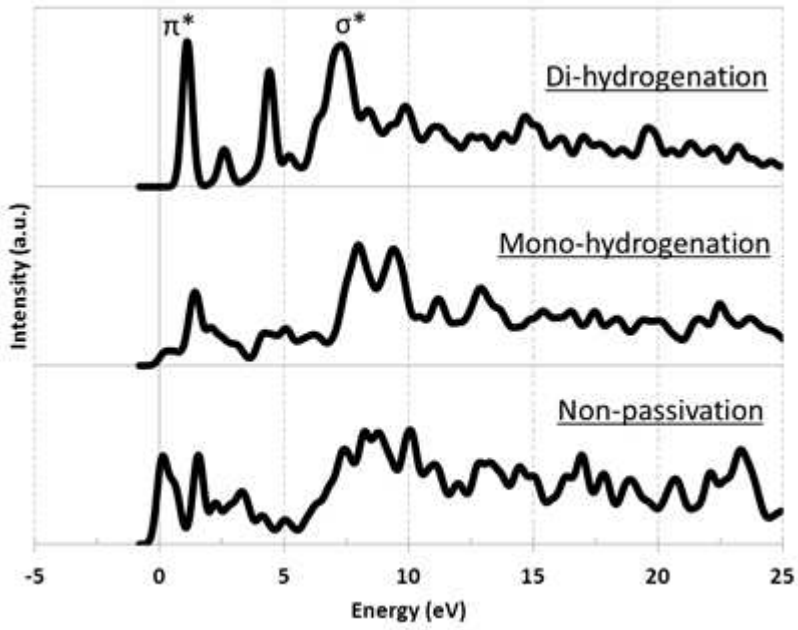

Figure 13: Effect of hydrogenation on the total core-loss EELS for a ZGNR.

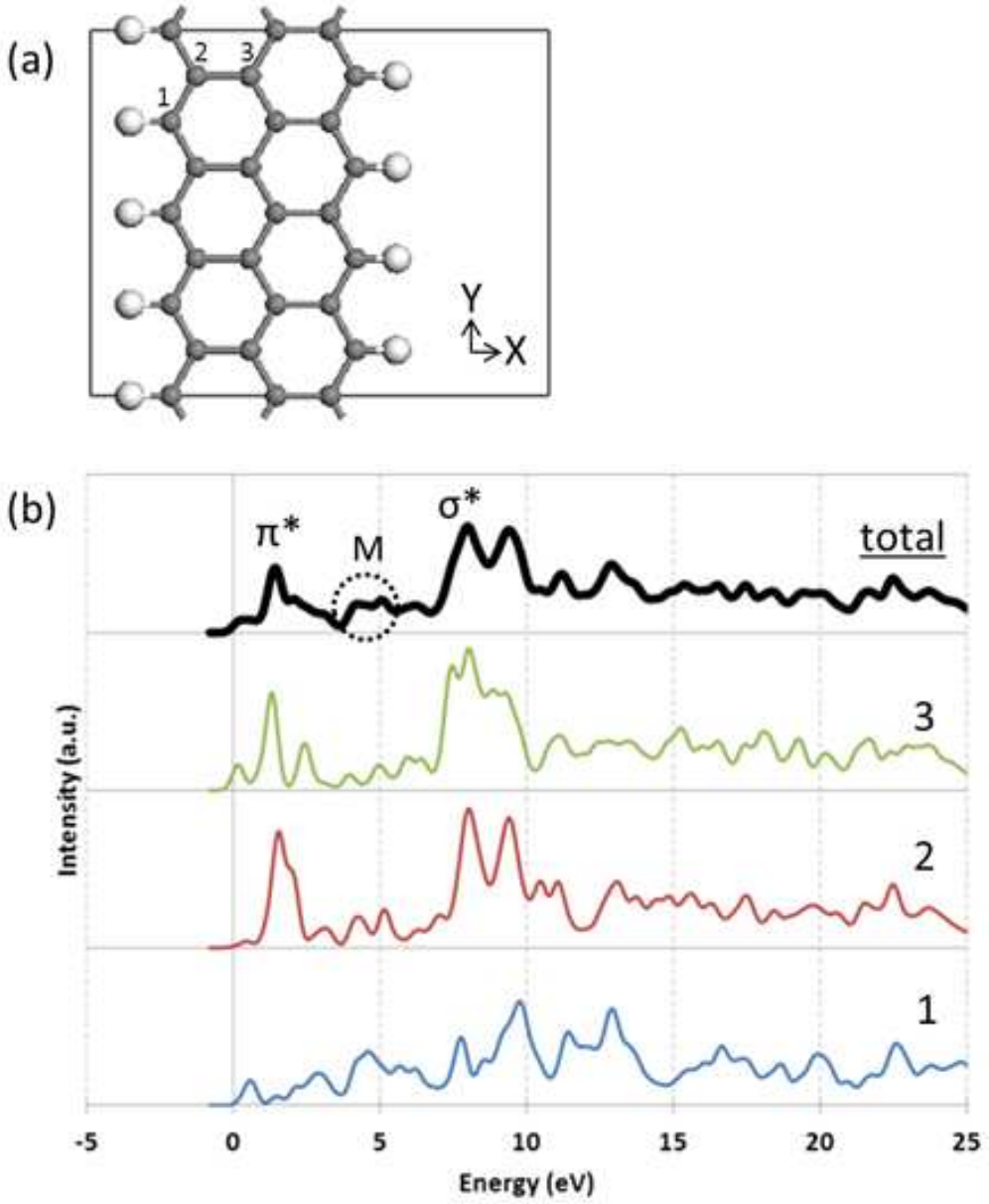

Figure 14: (Color online) Atom-resolved core-loss EELS for each of the distinct sites in a mono-hydrogenated ZGNR. (a) shows the labeling of each site and the coordinate system used. (b) shows the calculated core-loss EELS for a core-hole on the labelled carbon atom, and "total" shows the effect of averaging the core-loss EELS across all sites. There is a qualitatively new peak visible in the total core-loss EELS that is labelled M. See text for more discussion.

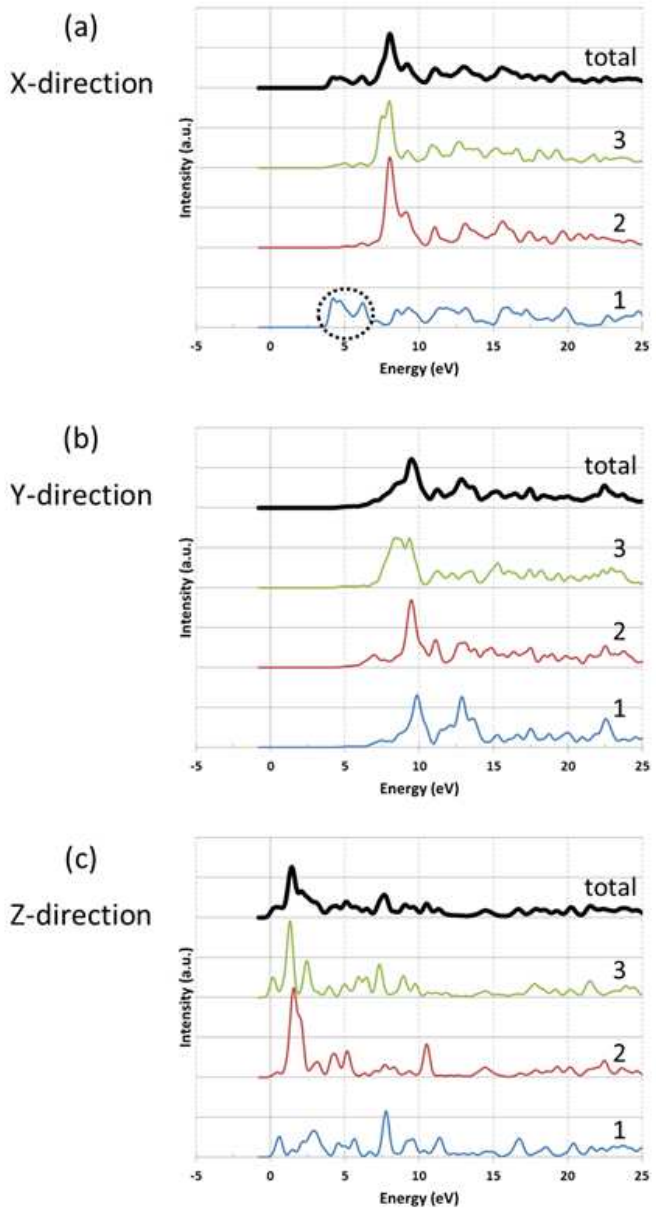

Figure 15: (Color online) Effect of polarized E-field on the atom-resolved core-loss EELS for each of the distinct sites in a mono-hydrogenated ZGNR. Parts (a), (b) and (c) shows the effect of incident E-field that is polarized in the X-, Y- and Z- direction respectively. A qualitatively new peak is seen at site 1 for X-polarization.

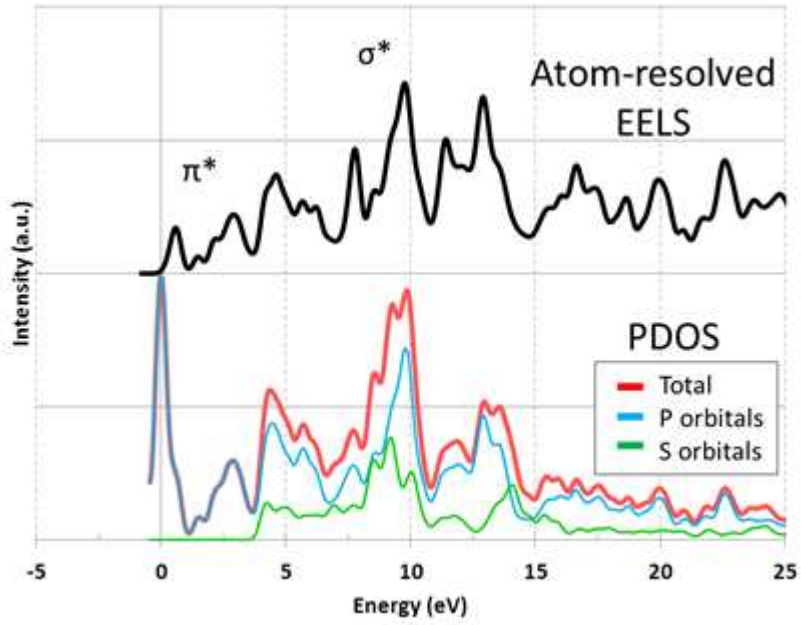

Figure 16: (Color online) Comparison of atom-resolved core-loss EELS (top) and the projected electronic density of states (bottom) for the edge site in mono-hydrogenated ZGNR. The PDOS makes a dominant contribution to the core-loss EELS spectrum and helps with the assignment of the symmetry of each peak.

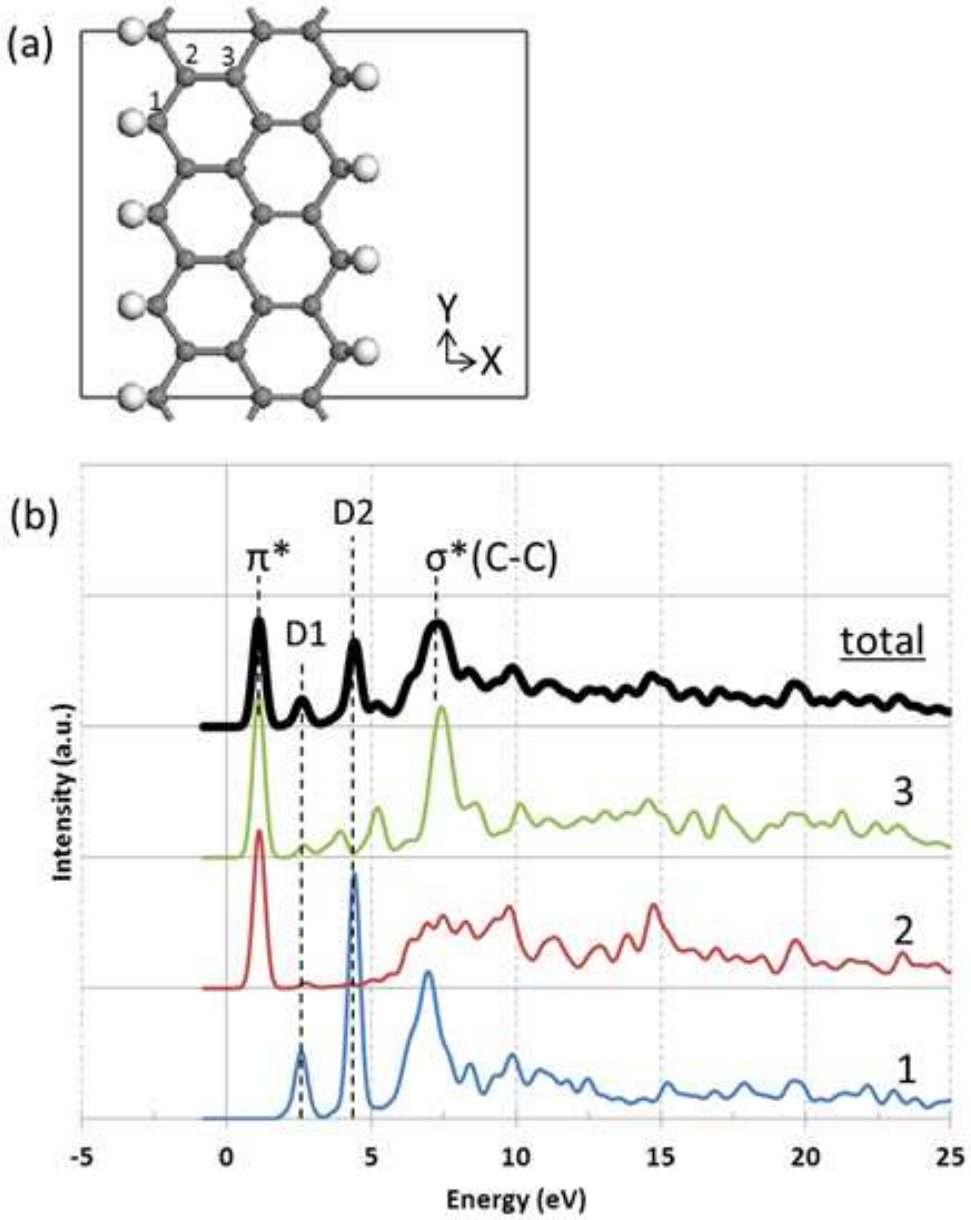

Figure 17: (Color online) Atom-resolved core-loss EELS for each of the distinct sites in a di-hydrogenated ZGNR. (a) shows the labeling of each site and the coordinate system used. (b) shows the calculated core-loss EELS for a core-hole on the labelled carbon atom, and "total" shows the effect of averaging the core-loss EELS across all sites. There are two new peak visible in the core-loss EELS for site 1 that are labelled as D1 and D2. See text for detailed discussion.

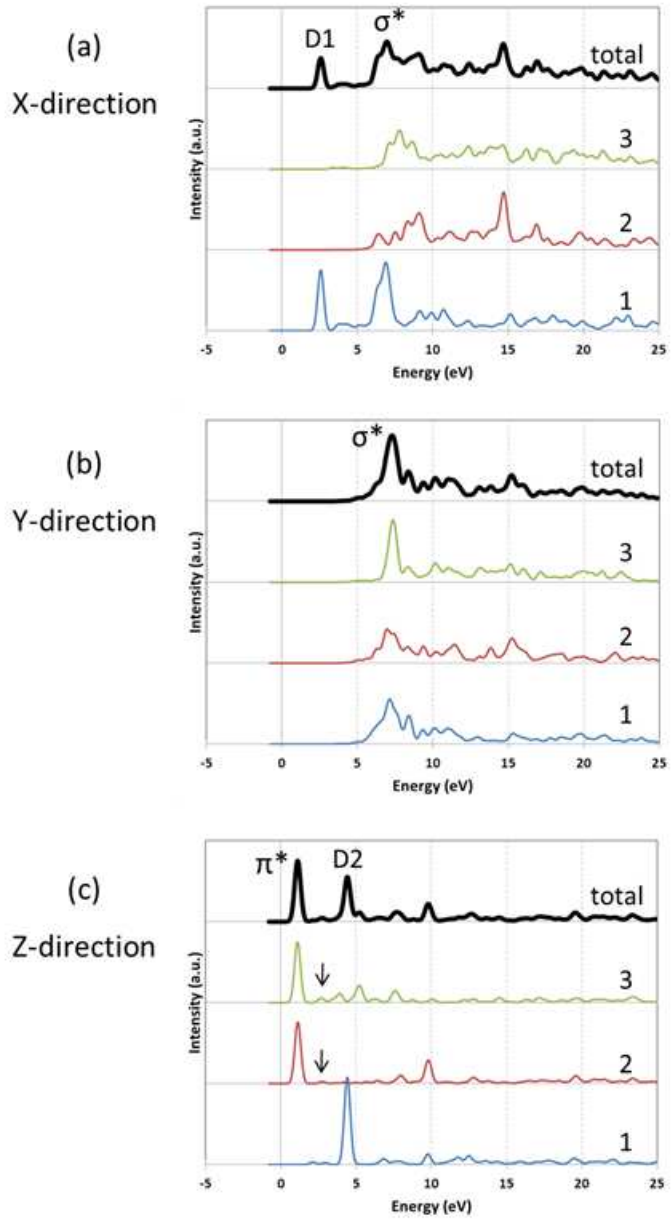

Figure 18: (Color online) Effect of polarized E-field on the atom-resolved core-loss EELS for each of the distinct sites in a mono-hydrogenated ZGNR. Parts (a), (b) and (c) shows the effect of incident E-field that is polarized in the X-, Y- and Z- direction respectively. Two qualitatively new peaks are seen at site 1 for X- and Z-polarization.

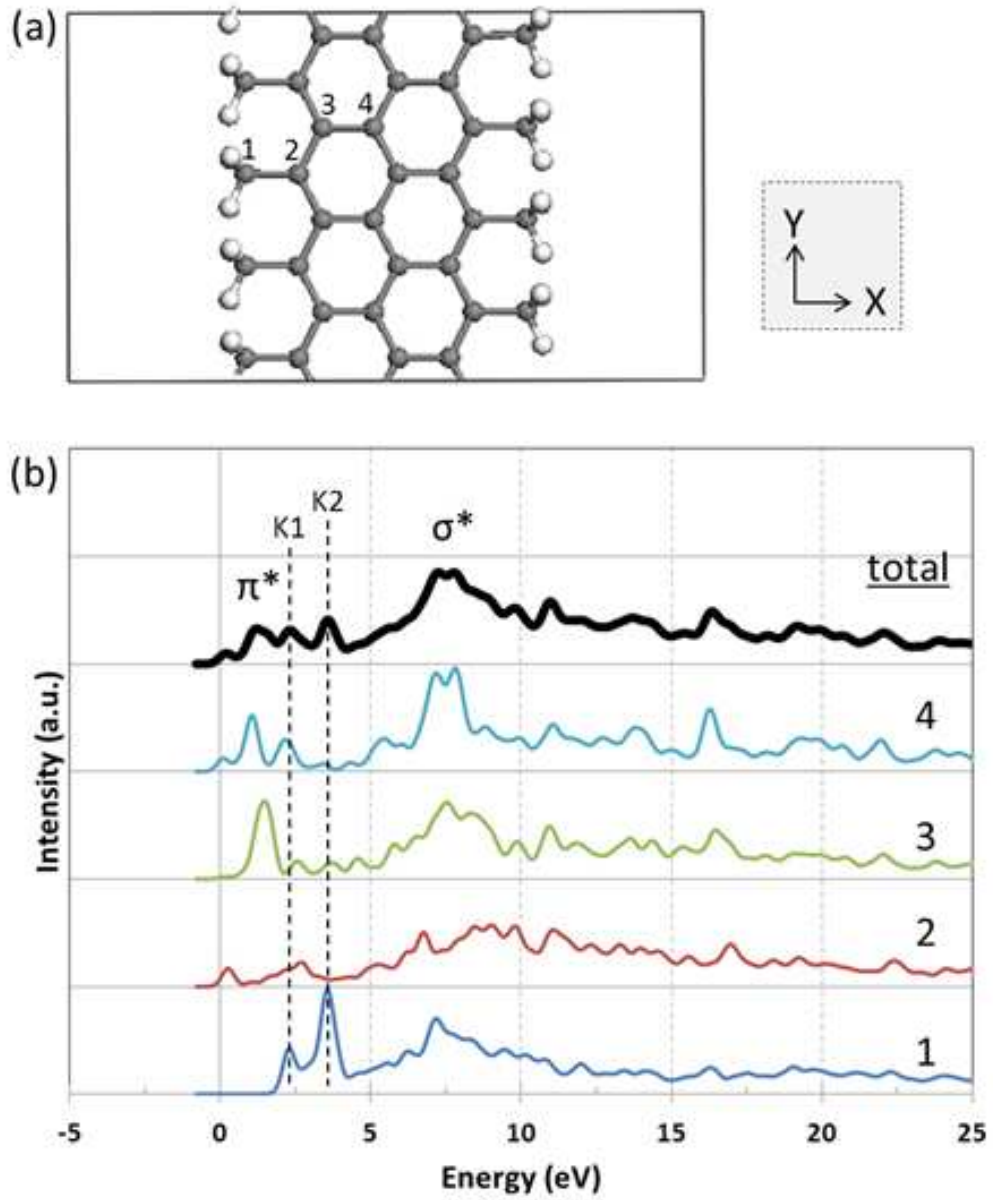

Figure 19: (Color online) Atom-resolved core-loss EELS for each of the distinct sites in a di-hydrogenated Klein-edge GNR. (a) shows the labeling of each site and the coordinate system used. (b) shows the calculated core-loss EELS for a core-hole on the labelled carbon atom, and "total" shows the effect of averaging the core-loss EELS across all sites. There are 2 new peaks visible in the core-loss EELS for site 1, that are labelled K1 and K2. See text for a detailed discussion.

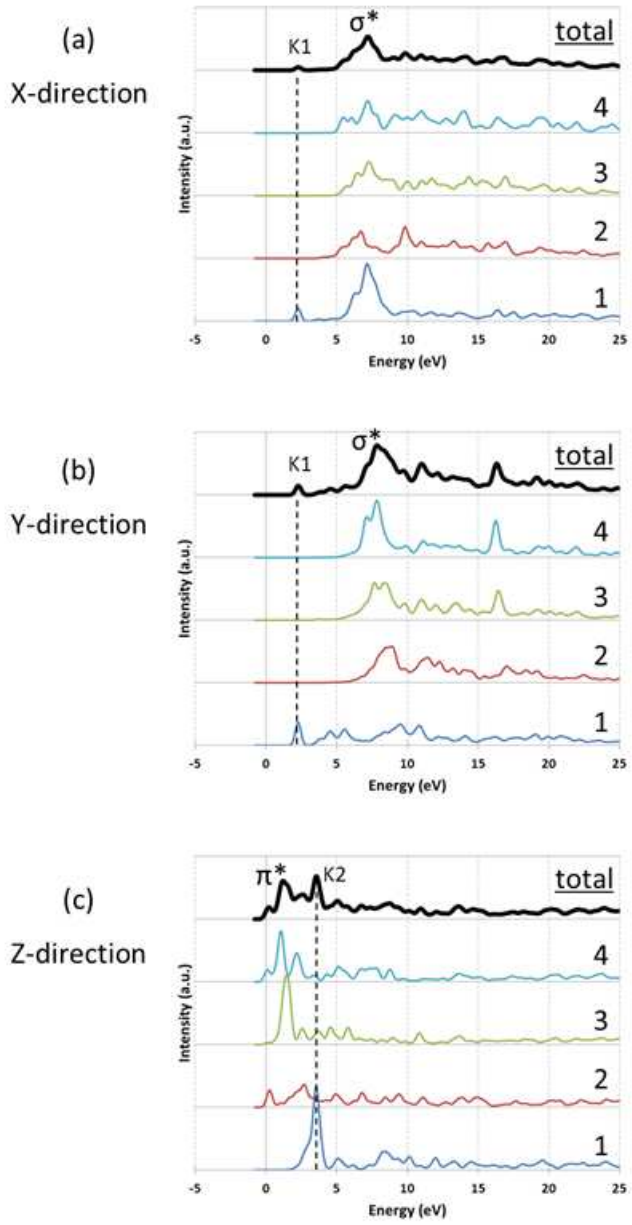

Figure 20: (Color online) Effect of polarized E-field on the atom-resolved core-loss EELS for each of the distinct sites in a mono-hydrogenated ZGNR. Parts (a), (b) and (c) shows the effect of incident E-field that is polarized in the X-, Y- and Z- direction respectively. Two qualitatively new peaks are seen at site 1.

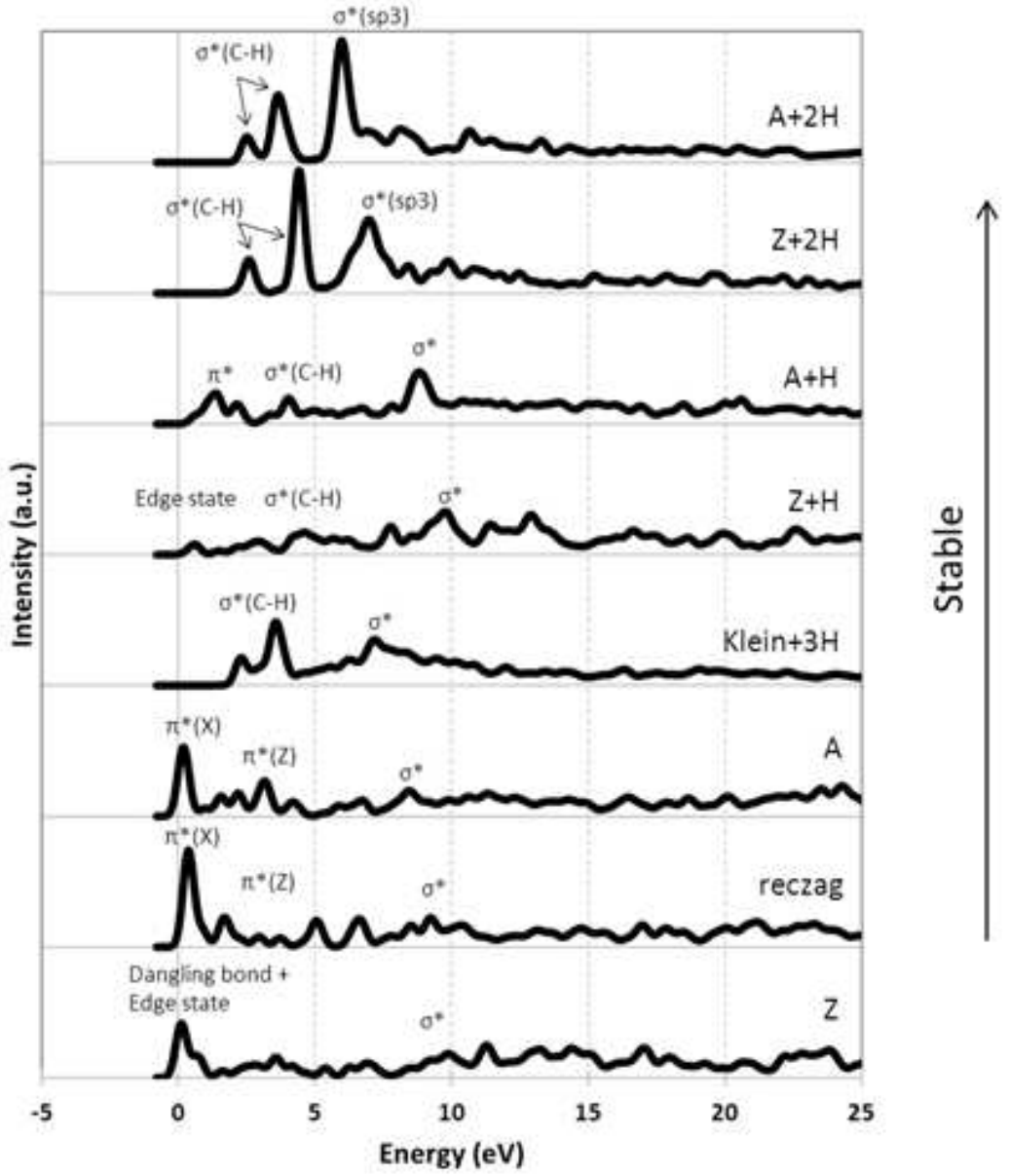

Figure 21: Effect of hydrogenation on the site-specific core-loss EELS for the edge carbon site in each of the different GNRs considered in this work. For brevity of labels, "A" refers to the unhydrogenated AGNR, "Z" to the unhydrogenated, unreconstructed ZGNR, "reczag" refers to the reconstructed zz-57 structure, "A+H" to the mono-hydrogenated AGNR, etc. Of the different Klein-edge structures, only the tri-hydrogenated Klein-edge GNR is included for clarity.